AGU ADVANCING EARTH AND SPACE SCIENCE

Geophysical Research Letters

RESEARCH LETTER
10.1029/2020GL089471

Antarctic Circumpolar Current Impacts on Internal Wave Life Cycles

S. Waterman[1], A. Meyer[2,3], K. L. Polzin[4], A. C. Naveira Garabato[5], and K. L. Sheen[6]

[1]Department of Earth, Ocean & Atmospheric Sciences, University of British Columbia, Vancouver, Canada, [2]Institute for Marine and Antarctic Studies, University of Tasmania, Hobart, TAS, Australia, [3]Australian Research Council Centre of Excellence for Climate Extremes, University of Tasmania, Hobart, TAS, Australia, [4]Woods Hole Oceanographic Institution, Woods Hole, MA, USA, [5]University of Southampton, National Oceanography Centre, Southampton, UK, [6]University of Exeter, Penryn, UK

Key Points:

- In situ observations show internal wave-like coherent features in the Antarctic Circumpolar Current
- Wave and background flow scales suggest that horizontal advection and wave-mean flow interactions are leading-order terms in wave evolution
- Features are detected where the background flow shear is large and where ray tracing calculations suggest a critical layer scenario

Supporting Information:

Supporting Information may be found in the online version of this article.

Correspondence to:

S. Waterman,
swaterman@eoas.ubc.ca

Citation:

Waterman, S., Meyer, A., Polzin, K. L., Naveira Garabato, A. C., & Sheen, K. L. (2021). Antarctic circumpolar current impacts on internal wave life cycles. *Geophysical Research Letters*, *48*, e2020GL089471. https://doi.org/10.1029/2020GL089471

Received 22 JUN 2020
Accepted 4 FEB 2021

Abstract Major gaps exist in our understanding of the pathways between internal wave generation and breaking in the Southern Ocean, with important implications for the distribution of internal wave-driven mixing, the sensitivity of ocean mixing rates and patterns to changes in the ocean environment, and the necessary ingredients of mixing parameterizations. Here we assess the dominant processes in internal wave evolution by characterizing wave and mesoscale flow scales based on full-depth in situ measurements in a Southern Ocean mixing hot spot and a ray tracing calculation. The exercise highlights the importance of Antarctic Circumpolar Current jets as a dominant influence on internal wave life cycles through advection, the modification of wave characteristics via wave-mean flow interactions, and the set-up of critical layers for both upward- and downward-propagating waves. Our findings suggest that it is important to represent mesoscale flow impacts in parameterizations of internal wave-driven mixing in the Southern Ocean.

1. Introduction

In the stratified ocean interior, turbulent mixing is primarily attributed to the breaking of internal waves. Currently, our understanding of this process is hampered by critical knowledge gaps concerning the pathways between internal wave generation and dissipation via wave breaking. These gaps are important to resolve for three key reasons: they determine how the spatial distribution of internal wave energy sources relate to that of internal wave-driven mixing; they impact the sensitivity of this mixing to changes in the wavefield environment; and they define the necessary ingredients of parameterizations of internal wave-driven mixing for general circulation models.

It is generally assumed that internal waves in the ocean interior have originated from the upper-ocean mixed layer or the ocean floor, forced by winds at the surface or by the flow of tidal or geostrophic motions over rough topography. In both cases, internal waves can propagate away from their generation site before breaking and generating mixing. Observations of turbulent dissipation and internal wave-scale flow properties provide strong support for the perception that breaking internal waves are important for turbulent dissipation and mixing in the Southern Ocean interior (Brearley et al., 2013; Cusack et al., 2017; Meyer et al., 2015; Sheen et al., 2013; St. Laurent et al., 2013; Waterman et al., 2013). Here, the contribution from bottom-sourced waves generated by the interaction of deep-reaching geostrophic jets and eddies with the bottom topography is thought to be especially significant (de Lavergne et al., 2016; Nikurashin & Ferrari, 2013).

There exist a number of thought-provoking results relating to internal wave-driven mixing in the Southern Ocean interior that raise important questions about the pathways to internal wave breaking in this unique environment. For example, theoretical predictions of the lee wave energy flux based on observed bottom flow speed, stratification, and topography have been found to overpredict the observed near-bottom turbulent dissipation rate seen in different regimes of the ACC (Cusack et al., 2017; Sheen et al., 2013; Waterman et al., 2013). Similarly, finescale parameterization predictions for the dissipation rate based on the observed rate of energy transfer at internal wave scales have been found to systematically overpredict the observed near-bottom turbulent dissipation rate in regions of bottom wave generation (Sheen et al., 2013; Takahashi & Hibiya, 2019; Waterman et al., 2014). In addition, off-bottom maxima in observed dissipation rate vertical

profiles in these regions (see Sheen et al., 2013; Waterman et al., 2013) do not match the vertical structure characteristically assumed in standard parameterizations for topographically-radiated internal wave-driven mixing (e.g., St. Laurent et al., 2002; Nikurashin & Ferrari, 2013).

A number of possible explanations for these thought-compelling mismatches have been suggested (Kunze & Lien, 2019), including the overestimation of the lee wave energy flux because of the poor representation of near-bottom flows and/or small-scale topography, and/or flow blocking and splitting (Klymak, 2018; Nikurashin et al., 2014; Trossman et al., 2015; Yang et al., 2018); remote dissipation due to the downstream advection or cross-stream propagation of internal wave energy (Kunze & Lien, 2019; Meyer et al., 2016; Zheng & Nikurashin, 2019); the absorption of wave energy by the mean flow through wave-mean flow interactions/wave action conservation (Kunze & Lien, 2019; Waterman et al., 2014); and sampling biases in a heterogeneous turbulent field (Klymak, 2018). A growing number of results point to the importance of the mesoscale flow in playing an order-one role in the observed discrepancies and setting the structure of wave-driven mixing in the ACC. For example, Zheng and Nikurashin (2019) suggest that the advection of internal waves by the mesoscale flow can significantly contribute to the reported difference between predicted wave generation and the observed energy dissipation. We observe significant differences in the average vertical profiles of wave and turbulent properties inside ACC jets versus outside ACC jets (Meyer et al., 2016; Sheen et al., 2013; Waterman et al., 2013). Furthermore, we find an association of finescale parameterization overprediction with large Froude numbers based on the vertical shear of the mesoscale flow (Sheen et al., 2013; Waterman et al., 2014). An association of prominent finescale parameterization overprediction with background flows with systematic backing tendency (Waterman et al., 2014), as well as systematic trends in vertical profiles of wave polarization, shear-to-strain variance and turbulent dissipation inside ACC jets (Sheen et al., 2013; Waterman et al., 2013), each suggest that critical layer dynamics may play a systematic role at these special sites. Consistent with this, Kunze and Lien (2019) argue that the transfer of lee wave energy back to the balanced flow through wave action conservation can account for a reduction in turbulent production by a factor of two, but note that this process appears insufficient to fully account for the discrepancy between turbulent dissipation and lee wave generation reported by Waterman et al. (2014). These varied results motivate further consideration of the implications of wave-mean flow interactions and other mesoscale flow influences on internal wave life cycles and, in turn, the magnitude and distribution of wave-induced mixing in this environment.

In this study, we exploit full-depth in situ measurements of internal wave-scale flow properties in a Southern Ocean mixing hot spot in which we expect elevated levels of internal wave activity owing to strong wind forcing and to the interaction of intense near-bottom flows with rough topography, as well as significant mesoscale flow influences associated with energetic ACC jets. We use these observations to identify and characterize both coherent internal wave-like signals, and the nature of these waves' background environment. Based on these characterizations, we evaluate the likely processes governing wave evolution through a characterization of timescales and a backward-in-time ray tracing calculation. Our work builds on that of Meyer et al. (2016), which characterized upper-ocean internal wave properties in this region using high-resolution hydrographic profiles from EM-APEX floats. Here, we extend this analysis using unique data in two significant ways: (1) expanding the wave characterization to full depth, allowing us to target bottom-generated waves closer to their generation site; and (2) probing plausible internal wave evolution pathways through a time-dependent ray tracing calculation in a realistic background flow and stratification environment.

2. Data and Methods

Our study is motivated by our identification of a number of coherent wave-like features in in situ observations from the Southern Ocean Finestructure (SOFine) project, conducted in 2008 on the northern flank of the Kerguelen Plateau in the Indian Ocean sector of the Southern Ocean. The survey site is characterized by the presence of multiple ACC frontal jets and moderately rough topography on horizontal scales of order 1–10 km. The jets' impingement on the topography is expected to be a strong local source of internal lee waves. In addition, strong wind forcing in the region is anticipated to be a significant surface source of near-inertial oscillations, which can then propagate into the ocean interior as near-inertial waves. Coherent wave-like features are identified both in the upper-ocean profiles of velocity and stratification collected by

EM-APEX floats deployed in the region (see Meyer et al., 2016), as well as in full-depth conductivity-temperature-depth (CTD) and lowered acoustic Doppler current profiler (LADCP) profiles acquired during a ship-board survey (discussed here). These latter observations provide a unique opportunity to characterize the wave-like signals in the deep ocean in terms of internal wave kinematics, and to consider their relationship with the topography, stratification, and background ACC flow. Full details on the survey site, survey observations and data processing are given in Waterman et al. (2013).

The full-depth profiles of the horizontal velocity anomaly and the neutral surface height anomaly are systematically examined for the presence of coherent wave-like features, which are positively identified if all of a number of criteria on the observed wave signal are satisfied; see Section S1 of the Supporting Information for full details. Wave properties are then characterized by assuming that the feature is an internal wave (as in, e.g., Meyer et al., 2016; Müller et al., 1978; Polzin, 2008) and applying linear wave theory; see Section S2 in the Supporting Information for a full description. In these calculations, we assume plane-wave internal waves propagating in a low Rossby number, Ro, low Froude number, Fr, geostrophically-balanced background flow correct to order (Ro, Fr) (see Polzin et al., 1996, for a discussion). To characterize properties of the background flow and stratification environment in which the coherent wave features are observed, CTD, and LADCP profiles, as well as the satGEM projection (Meijers et al., 2011), are used. satGEM is a gravest empirical mode (GEM) projection of temperature and salinity fields in the Southern Ocean that, when combined with satellite altimetry, produces time-evolving temperature, salinity and velocity fields that approximate the mesoscale flow. The local background flow field is defined by smoothed variants of the measured velocity component vertical profiles, and the local background stratification is estimated via the adiabatic leveling method of Bray and Fofonoff (1981) applied to the measured *stratification* profile: see Section S3 in the Supporting Information for details. A comparison of the observed SOFine velocity profiles to those of the satGEM at relevant times and locations produces reasonable mesoscale structure agreement, endorsing our use of the satGEM product to provide background flow and stratification information at times and places where it is unavailable in the SOFine survey observations. The scales characterizing the wave features and the background flow and stratification environment through which they propagate and evolve are then combined to characterize timescales that indicate the relative importance of various processes influencing wave evolution from the perspective of wave action: see Section 3.3 and Section S4 in the Supporting Information for details. Finally, the life history of observed waves is considered via a ray tracing calculation (e.g., Lighthill, 1978; Olbers, 1981; Sheen et al., 2015) using the satGEM projections to provide the time- and space-varying background flow and stratification fields. Full details of the calculation are provided in Section S5 in the Supporting Information.

3. Results

3.1. Wave Characteristics

Based on the criteria defined in Section S1, we identify 7 downward-propagating and 14 upward-propagating coherent wave-like features in the 59 vertical profiles of LADCP and CTD observations. These wave-like features are commonly observed in the vicinity of the ACC frontal jets and/or in the eastern half of the survey domain (Figure 1); the latter is characterized by significantly rougher topography (see Waterman et al., 2013, their Figure 2). Downward-propagating waves are observed exclusively at depths ranging from 1,000 to 1,500 m. Upward-propagating waves are observed at a wide range of depths and heights above bottom, but are typically found within 500–1,500 m of the seafloor (Table S1). Median-wave scales computed as described in Section S2 characterize the downward-propagating waves as having typical vertical wavelengths of ∼140 m and horizontal wavelengths of ∼8 km. Upward-propagating waves are characterized as having vertical wavelengths of ∼120 m and horizontal wavelengths of ∼2 km. Significant variation among the individual features observed does exist, particularly in the vertical wavelength and frequency for upward-propagating waves (see Table S1 for standard deviations in wave properties). Downward-propagating waves exhibit a narrow range of intrinsic frequencies, all less than $1.25f$, where f is the local Corilois frequency. In contrast, upward-propagating waves have a much wider range of frequencies, with 5 of 14 waves having intrinsic frequencies greater than $2f$ (Figure 1).

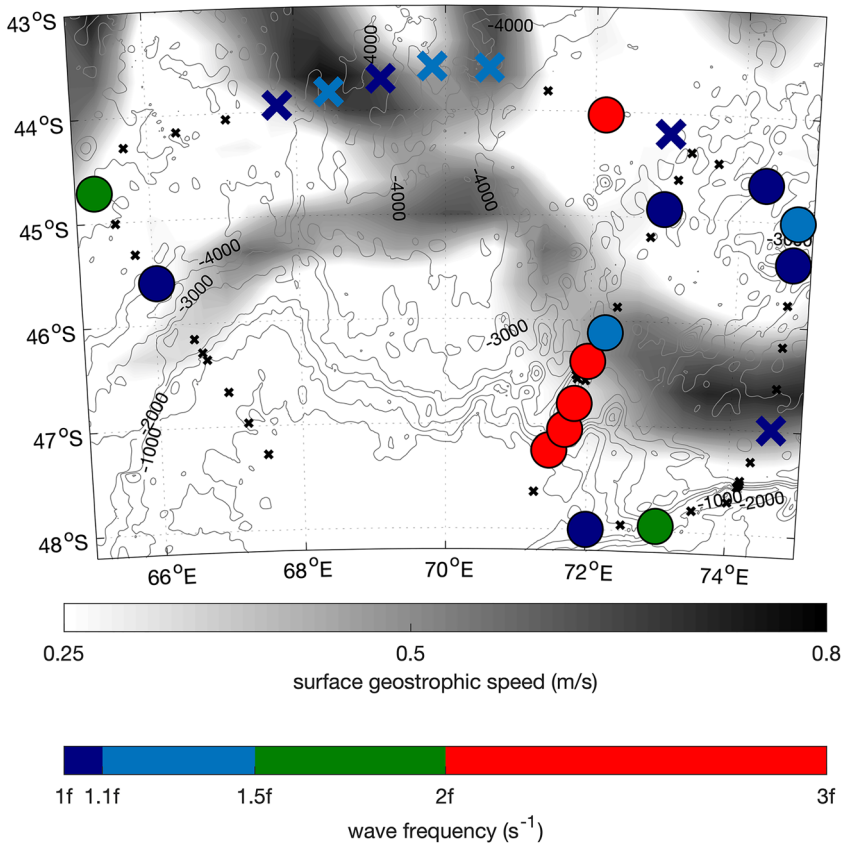

Figure 1. Location of observed coherent wave-like features (circles and enlarged **x**s), their direction of propagation (downward-propagating denoted by an **x**, upward-propagating by a circle), and their intrinsic frequency (color). For reference, the SOFine survey-mean surface geostrophic speed in the region computed from the Ssalto/Duacs altimeter products produced and distributed by the Copernicus Marine and Environment Monitoring Service (CMEMS) (http://www.marine.copernicus.eu) is shown in gray shading to outline the location of the ACC frontal jets during the survey period. Gray contours show the regional bathymetry in 500 m intervals from Smith and Sandwell ship-sounding bathymetry (Smith & Sandwell, 1997). Small black "x"s show the SOFine survey stations (refer to Waterman et al., 2013 for a full description of the SOFine survey).

3.2. Background Environment

As already noted, the coherent wave-like features are typically observed in the vicinity of the ACC frontal jets that transected the survey domain. As such, background horizontal flow speeds at the locations of observed wave packets are typically moderate to large: 22 cm s^{-1} on average for downward-propagating waves, and 8 cm s^{-1} on average for upward-propagating waves. Background flow speeds are on average 10x larger than the diagnosed intrinsic horizontal group speeds of the downward-propagating waves; they are 7x larger on average than the inferred horizontal group speeds of the upward-propagating features. Large background flow horizontal speeds, combined with the horizontal wave scales estimated from the observed shear-to-strain ratio and velocity-buoyancy phase, imply significant mean flow-induced Doppler shifting of the waves' frequencies: median amplitudes of 1.0*f* for downward-propagating waves, and 0.8*f* for upward-propagating waves (Table S1).

Potentially important for these waves' evolution is the nature of the background flow's vertical shear, strain, and vorticity, expected to be elevated in the vicinity of ACC jets. LADCP measurements permit an in situ characterization of the larger-scale vertical shear in the vicinity of the coherent features identified (Table S1 and Figure 2). We find that downward-propagating features are always identified in positively-signed vertical shear (corresponding to decreasing background speed magnitude with depth), typically at depths that correspond to a transition from a more rapid decrease of background flow speed with depth above to a much more gradual decrease of background flow speed with depth below (Figure 2a). Upward-propagating

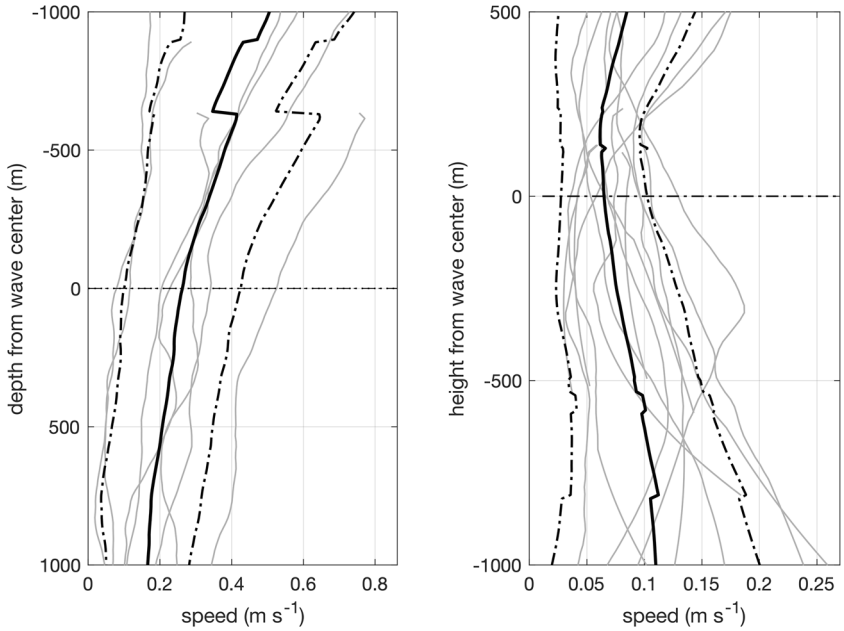

Figure 2. Background flow profiles in the vicinity of coherent wave-like features identified for all downward-propagating (left) and upward-propagating (right) features (light gray lines). The mean of all profiles is shown by the thick solid black line. The mean ± one standard deviation of the mean is shown by the thick dash-dotted black lines. Profiles are each centered around the observed depth/height of the feature. Discontinuities in the mean and mean ± standard deviation profiles arise from changes in the number of profiles being averaged, a consequence of the profiles having differing "depth from wave" extent.

coherent wave-like features are also characteristically observed near a transition in the background flow profile, with negatively-signed vertical shear (corresponding to an increase of background speed with depth toward the bottom) below and near-zero or positive vertical shear above (Figure 2b). Median magnitudes of vertical shear in the background flow in the vicinity of the features are small: $0.02N$ for downgoing waves and $0.03N$ for upgoing features respectively (Table S1), where N is the local background (i.e., adiabatically-leveled) value of the buoyancy frequency. The satGEM product permits estimation of the large-scale flow strain and vorticity in the vicinity of identified features: we find median magnitudes of $0.1f$ and $0.1f$ for downward-propagating waves, and $0.06f$ and $0.02f$ for upward-propagating waves respectively (Table S1). These values are modest, but likely biased low by the coarse effective spatial resolution of the altimetric measurements (see, e.g., Arbic et al., 2014). Elevated values of strain over vorticity imply that satGEM-derived estimates of the Okubo-Weiss parameter of the background flow are typically positive for both upward- and downward-propagating features (5 of 7 and 12 of 14 cases, respectively). Assuming that these estimates serve as an indication of similarly-elevated rate-of-strain at unresolved scales (e.g., Siegelman et al., 2020), in this scenario, we expect the azimuth of the horizontal wave vector to asymptotically point toward a direction solely determined by the geostrophic velocity gradient, and the magnitude of the wave vector to exhibit exponential growth. Under these conditions, wave capture (Bühler & McIntyre, 2005) or the shrinking catastrophe (Jones, 1969) may play a significant role in the wave evolution. These processes serve as plausible explanations for the large-amplitude wave-like features we observe.

3.3. Wave Evolution

To gain insight into what the observed wave, background flow and stratification scales imply for the relative importance of processes expected to drive wave evolution, we examine related timescales linked to the evolution of wave action. Specifically, we consider the timescales characterizing:

1. the time-rate-of-change of wave action due to advection by the subinertial flow; this defines the advection timescale, $\tau_{\text{advection;}}$

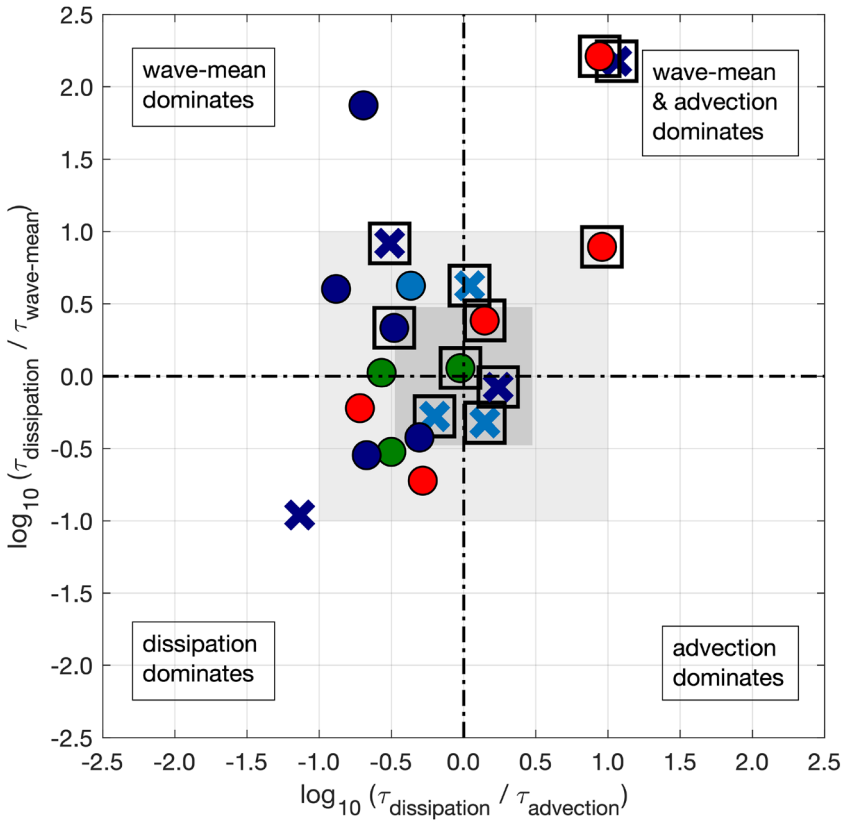

Figure 3. A comparison of the scale estimates of select timescales for all coherent wave-like features informing on the relative importance of various processes in driving the timeevolution of wave action. The wave-mean timescale displayed is the shortest of the set of three timescales associated with the time evolution of the k, l, and m wavenumber components respectively. As in Figure 1, downward-propagating features are denoted by Xs and upward-propagating features by circles, and symbols are colored by their intrinsic wave frequency. Stations inside ACC frontal jets are enclosed in black squares. Gray boxes indicate where in the plot-space timescales characterizing advection and wave-mean flow interaction are within a factor of 3 of the dissipation timescale (dark gray) and where these timescales are the same order of magnitude as the dissipation timescale (light gray).

2. the time-rate-of-change of wave action due to refraction associated with the changing "background" medium, that is, due to subinertial flow shears and variations in the background stratification; this defines three timescales of wave-mean flow interaction, $\tau_{\text{wave-mean k}}$, $\tau_{\text{wave-mean l}}$ and $\tau_{\text{wave-mean m}}$ corresponding to the rate of refraction of each of the three components of the wavevector; and
3. the time-rate-of-change of wave action due to dissipation; this defines the dissipative timescale, $\tau_{\text{dissipation}}$.

The magnitude of these timescales is set by (1) the magnitude of the background flow velocity and the characteristic length scale of horizontal variations in wave action (here assumed to be the first baroclinic Rossby deformation radius); (2) the various wavenumber components and the magnitude of the background current shears and stratification gradient; and (3) under various assumptions (see Section S4), the rate of turbulent dissipation, ϵ, and the wave packet total energy. We compute scale estimates using our characterizations of the wave properties (Section 3.1) and the background flow and stratification environment (Section 3.2), combined with microstructure-derived estimates of ϵ (see Waterman et al., 2013): see Section S4 in the Supporting Information for full details. We then compare these scale estimates to gain insight into the dominant (shortest timescale) processes driving the time evolution of wave properties.

The timescale characterization (Table S1 and Figure 3) suggests a leading-order role of mesoscale flow processes in wave evolution inside the ACC. Timescales associated with background flow advection and/or wave-mean flow interaction are of the same order of magnitude or shorter than corresponding dissipation timescales in almost all cases (20 out of 21 features). Further, advection and/or wave-mean flow interaction

dominate over dissipation (i.e., are characterized by a shorter timescale) in 67% of cases. Stations inside the ACC frontal jets (enclosed by black squares in Figure 3) consistently have advection and wave-mean flow interaction timescales that suggest these processes modify wave action at a comparable (to within a factor of 3) or faster rate relative to dissipation. Notably, all five features for which dissipation dominates (i.e., for which the dissipation timescale is the shortest by more than a factor of 3) are from stations outside the ACC jets.

Further insights into the potential influences of the ACC on wave evolution are provided by a backwards-in-time ray tracing calculation (see Section S5), which quantifies plausible large-scale flow impacts on wave evolution in the absence of wave-wave interactions and dissipation. These calculations illustrate the role of the mesoscale flow in steering and extending the trajectories of the modeled wave packets (Figure 4a), in particular for a majority of downward-propagating features which often follow the mesoscale flow. These features are tracked back to the base of the mixed layer in 2–12 days over which they travel a median distance of 160 km; during this time the background flow speed typically exceeds the intrinsic horizontal propagation of the wave feature by approximately an order of magnitude. The background flow also dominates over horizontal intrinsic wave propagation for upward-propagating features however, these waves, which have a much wider span of modeled ages at the time of observation ranging from 0.1 to 21 days, typically travel much shorter horizontal distances from their presumed generation site (the median value for the distance traveled by upward-going features over the ray-tracing integration is only 9 km). Features with the shortest ages at the time of observation cluster in the southeastern part of the survey domain where the topography is rough and the water depth is relatively shallow (Figure 1). Here, timescale analysis based on the observed rates of dissipation suggests that dissipation is the dominant process in these waves' time evolution.

The ray-tracing calculation further highlight a second potentially-important influence of the ACC on wave evolution: that of changing the wave properties through wave-mean flow interaction, specifically via wavenumber refraction associated with the background flow shear. For the majority of cases (all downward-propagating features and 9 of 14 upward-propagating features), this interaction forces a wavenumber evolution toward smaller aspect ratio, both via an increase in the vertical wavenumber component and a decrease in the horizontal wavenumber component. As a consequence, these waves exhibit a common evolution from higher-frequency and a more vertical trajectory early in their life cycle (near the surface or near the bottom) to a frequency that approaches f and a trajectory that approaches horizontal at the time of observation (Figures 4b and 4c). Interestingly, it is the modulation of the horizontal wavenumber magnitude that is the primary driver of the decrease in intrinsic frequency in most cases. This evolution is consistent with the waves approaching a critical layer scenario in both downward- and upward-propagating cases, and these dynamics thus further provide a plausible mechanism that would amplify wave amplitude and thus promote the feature's detection in the observational data. In summary, these calculations indicate that the ACC shear, and the critical layer situations that it can set up for both upward- and downward-propagating waves, may play an important role in setting the vertical profile of internal wave energy and, ultimately, internal wave-driven dissipation and mixing.

4. Summary and Discussion

In this study, we use in situ and satellite-derived measurements in a Southern Ocean mixing hot spot to characterize the scales of observed coherent internal wave-like features and the nature of these features' background environment, and further to consider the dominant processes in the waves' time evolution. Our results highlight the potential for the ACC to play a leading-order role in wave evolution through advection and wave-mean flow interaction. Furthermore, they suggest that our observations of large-amplitude coherent wave-like features plausibly stem from the approach to a critical layer, and/or scenarios of wave capture or shrinking catastrophe. Overall, our findings suggest that the ACC may play a significant role in shaping the vertical profiles of internal wave-driven dissipation and mixing, connecting sites of internal wave generation and breaking, and modulating the relationship between the internal wave energy flux and the local turbulent dissipation rate.

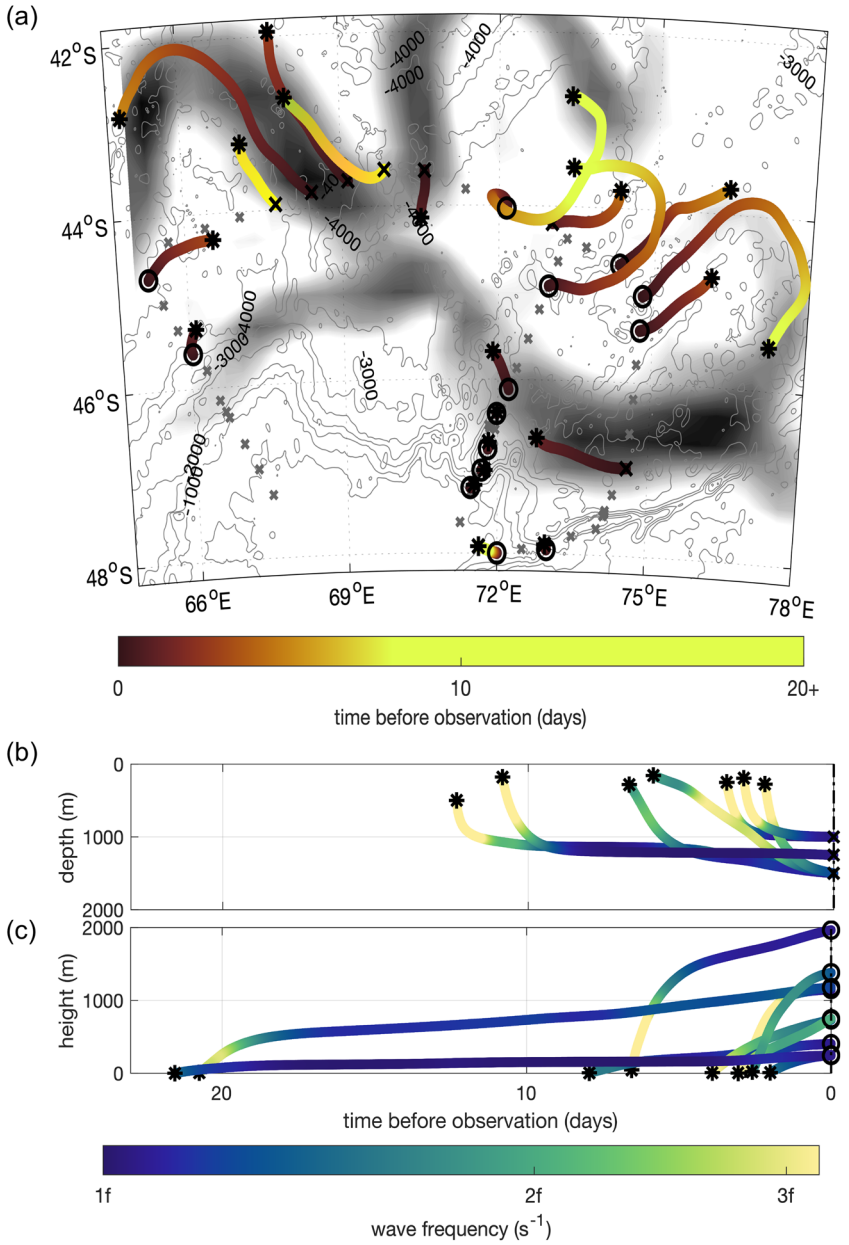

Figure 4. Plausible life histories of observed coherent wave-like features from backwards-in-time linear ray tracing calculation. (a) Horizontal trajectories of the modeled wave packets colored by time before observation. Xs indicate locations where downward-propagating features are observed, open circles indicate locations where upward-propagating features are observed, and asterisks indicate the locations where the backwards-in-time modeled wave packet reaches the base of the mixed layer or the seafloor. Mean surface geostrophic speed, regional bathymetry and survey stations are indicated as in Figure 1. Depth-time trajectories for (b) downward-propagating features and (c) select upward-propagating features. Here Xs indicate the depths where downward-propagating features are observed, open circles indicate the heights above the seafloor where upward-propagating features are observed, and asterisks indicate the time before observation that the backwards-in-time modeled wave packet reaches the base of the mixed layer or the seafloor. In panels (b) and (c) the trajectories are colored by the modeled intrinsic frequency of the wave packet as a function of time.

This work has several important limitations that need to be taken into consideration when assessing the implications of our results. First, with only a single hydrographic profile and a single velocity profile to characterize each wave feature, confidence limits on the estimated internal wave characteristics are unknown. Second, our knowledge of the three-dimensional background flow environment, based on the satGEM

fields, is coarsely-resolved and subject to a number of assumptions. Of particular relevance is the expectation that the satGEM fields are likely to underestimate the influence of horizontal strain and vorticity on the waves' evolution. Third, the simple linear ray tracing model employed here does not account for the effects of nonlinear wave-wave interactions or turbulent dissipation, nor does it capture the full range of wave-mean flow interactions at play in such a complex system. With respect to the latter, there are a number of scenarios in which the assumptions inherent to our linear ray tracing calculation may be violated, for example, in situations where the Wentzel-Kramers-Brillouin (WKB) approximation breaks down (e.g., Nault & Sutherland, 2008), where large-amplitude effects associated with the interaction of the waves and the wave-induced mean flow become significant (e.g., Brown et al., 2008), and, of particular relevance, where waves are evolving toward critical layer scenarios (see, e.g., Booker & Bretherton, 1967; Jones, 1969; Olbers, 1981; Whitt & Thomas, 2013). Furthermore, our formulation neglects additional processes such as instability mechanisms that may be important in transferring energy from larger-scale motions to dissipation scales (e.g., Thomas & Taylor, 2014). Finally, these observations are from a spatially-confined region in the Southern Ocean, and the applicability of these dynamics to the Southern Ocean generally remains an open question.

Given these limitations, it is appropriate to consider these characterizations of the wavefield, the background flow environment and its influence on wave dynamics presented here as plausible scale estimates, and the ray tracing exercise to consider wave evolution as a heuristic technique. Confidence in our wave parameter characterization is provided by the study of Meyer et al. (2016), Meyer et al. 2016, by virtue of using EM-APEX float profile data in the region, have the luxury of exploiting consecutive profiles to characterize a single wave-like feature, and as such can estimate uncertainty in their derivation of wave parameters. They report that estimated uncertainties are small, and do not alter the interpretation of their results. Furthermore, they document median wave parameters of similar scales to those reported here, within one mean standard deviation. Future observations targeting the assessment of wave properties and their local environment will be important to establish robustness of the characterizations presented here. We further recommend that the various effects and mechanisms not included in the simple linear ray tracing calculation discussed above be carefully considered in future work to determine whether their inclusion has a qualitative impact on findings presented here. Given that large rate-of-strain in the mesoscale flow is likely to play an important role in focusing wave-mean flow interaction, we specifically recommend that mesoscale rate-of-strain modulation of wave-mean flow interactions be explored in future with an appropriate data set.

Despite the above limitations and the need for further investigation, we argue that the big picture lessons suggested by the plausible scale estimates presented in this work are useful in guiding ongoing research efforts on internal wave-driven mixing. Specifically, the identification of additional pathways and fates for internal wave energy suggested here may provide valuable perspectives from which to better understand the emerging relationships between spatial maps of internal wave energy sources and internal wave-driven dissipation and mixing (e.g., de Lavergne et al., 2019; Waterhouse et al., 2014), as well as the mismatches between our theoretical descriptions of the internal wavefield and the distribution of turbulent dissipation identified in various recent studies (e.g., Cusack et al., 2017; Nikurashin et al., 2014; Sheen et al., 2013; Takahashi & Hibiya, 2019; Waterman et al., 2013, 2014; further see Section S6 in the Supporting Information). By suggesting a plausible mesoscale flow modulation of the internal wave-driven mixing profile in this region, our results argue for a need to consider mesoscale flow influences in internal wave-driven mixing parameterizations.

Acknowledgments
The authors wish to thank the officers, crew, and scientific compliment aboard the RRS James Cook during cruise JC029. The SOFine project was funded by the UK Natural Environmental Research Council (NERC) (grant NE/G001510/1). S. Waterman is currently supported by the National Science and Engineering Research Council of Canada (NSERC) Discovery Grant Program (NSERC-2020-05799). A. Meyer acknowledges current support from the ARC Centre of Excellence for Climate Extremes (CE170100023) and previous support from the joint CSIRO-University of Tasmania Quantitative Marine Science (QMS) program. A. N. Garabato acknowledges the support of the Royal Society and the Wolfson Foundation.

Data Availability Statement

The data used in the preparation of this manuscript are available on request from the British Oceanographic Data Centre (http://www.bodc.ac.uk).

References

Arbic, B. K., Müller, M., Richman, J. G., Shriver, J. F., Morten, A. J., Scott, R. B., et al. (2014). Geostrophic turbulence in the frequency-wavenumber domain: Eddy-driven low-frequency variability. *Journal of Physical Oceanography*, *44*, 2050–2069. https://doi.org/10.1175/JPO-D-13-054.1

Booker, J. R., & Bretherton, F. P. (1967). The critical layer for internal gravity waves in a shear flow. *Journal of Fluid Mechanics*, *27*, 513–539.
Bray, N. A., & Fofonoff, N. P. (1981). Available potential energy for MODE eddies. *Journal of Physical Oceanography*, *11*, 30–47.
Brearley, J. A., Sheen, K. L., Naveira Garabato, A. C., Smeed, D. A., & Waterman, S. (2013). Eddy-induced modulation of turbulent dissipation over rough topography in the Southern Ocean. *Journal of Physical Oceanography*, *43*, 2288–2308. https://doi.org/10.1175/JPO-D-12-0222.1
Brown, G. L., Bush, A. B. G., & Sutherland, B. R. (2008). Beyond ray tracing for internal waves. II. Finite-amplitude effects. *Physics of Fluids*, *20*, 106602. https://doi.org/10.1063/1.2993168
Bühler, O., & McIntyre, M. E. (2005). Wave capture and wave-vortex duality. *Journal of Fluid Mechanics*, *534*, 67–95. https://doi.org/10.1017/S0022112005004374
Cusack, J. M., Naveira Garabato, A. C., Smeed, D. A., & Girton, J. B. (2017). Observation of a large lee wave in the Drake Passage. *Journal of Physical Oceanography*, *47*, 793–810. https://doi.org/10.1175/JPO-D-16-0153.1
de Lavergne, C., Falahat, S., Madec, G., Roquet, F., Nycander, J., & Vic, C. (2019). Toward global maps of internal tide energy sinks. *Ocean Modelling*, *137*, 52–75. https://doi.org/10.1016/j.ocemod.2019.03.010
de Lavergne, C., Madec, G., Le Sommer, J., Nurser, A. J. G., & Naveira Garabato, A. C. (2016). The impact of a variable mixing efficiency on the abyssal overturning. *Journal of Physical Oceanography*, *46*, 663–681. https://doi.org/10.1175/JPO-D-14-0259.1
Jones, W. L. (1969). Ray tracing for internal gravity waves. *Journal of Geophysical Research*, *74*, 2028–2033.
Klymak, J. M. (2018). Non-propagating form drag and turbulence due to stratified flow over large-scale abyssal hill topography. *Journal of Physical Oceanography*, *48*, 2383–2395. https://doi.org/10.1175/JPO-D-17-0225.1
Kunze, E., & Lien, R.-C. (2019). Energy sinks for lee waves in shear flow. *Journal of Physical Oceanography*, *49*, 2851–2865. https://doi.org/10.1175/JPO-D-19-0052.1
Lighthill, J. (1978). *Waves in fluids* (p. 540.): Cambridge University Press.
Müller, P., Olbers, D. J., & Willebrand, J. (1978). The Iwex spectrum. *Journal of Geophysical Research*, *83*, 479–500.
Meijers, A. J. S., Bindoff, N. L., & Rintoul, S. R. (2011). Frontal movements and property fluxes: Contributions to heat and freshwater trends in the Southern Ocean. *Journal of Geophysical Research*, *116*, C08024. https://doi.org/10.1029/2010JC006832
Meyer, A., Polzin, K. L., Sloyan, B. M., & Phillips, H. E. (2016). Internal waves and mixing near the Kerguelen Plateau. *Journal of Physical Oceanography*, *46*, 417–437. https://doi.org/10.1175/JPO-D-15-0055.1
Meyer, A., Sloyan, B. M., Polzin, K. L., Phillips, H. E., & Bindoff, N. L. (2015). Mixing variability in the Southern Ocean. *Journal of Physical Oceanography*, *45*, 966–987. https://doi.org/10.1175/JPO-D-14-0110.1
Nault, J. T., & Sutherland, B. R. (2008). Beyond ray tracing for internal waves. I. Small-amplitude anelastic waves. *Physics of Fluids*, *20*, 106602. 10.1063/1.2993168
Nikurashin, M., & Ferrari, R. (2013). Overturning circulation driven by breaking internal waves in the deep ocean. *Geophysical Research Letters*, *40*, 3133–3137. https://doi.org/10.1002/grl.50542
Nikurashin, M., Ferrari, R., Grisouard, N., & Polzin, K. (2014). The impact of finite-amplitude bottom topography on internal wave generation in the Southern Ocean. *Journal of Physical Oceanography*, *44*, 2938–2950. https://doi.org/10.1175/JPO-D-13-0201.1
Olbers, D. J. (1981). The propagation of internal waves in a geostrophic current. *Journal of Physical Oceanography*, *11*, 1224–1233.
Polzin, K. L. (2008). Mesoscale eddy-internal wave coupling. Part I: Symmetry, wave capture, and results from the Mid-Ocean Dynamics Experiment. *Journal of Physical Oceanography*, *38*, 2556–2574. https://doi.org/10.1175/2008JPO3666.1
Polzin, K. L., Oakey, N. S., Toole, J. M., & Schmitt, R. W. (1996). Fine structure and microstructure characteristics across the northwest Atlantic Subtropical Front. *Journal of Geophysical Research*, *101*, 14111–14121.
Sheen, K. L., Brearley, J. A., & Naveira Garabato, A. C. (2013). Rates and mechanisms of turbulent dissipation and mixing in the Southern Ocean: Results from the Diapycnal and Isopycnal Mixing Experiment in the Southern Ocean (DIMES). *Journal of Geophysical Research: Oceans*, *118*, 2774–2792. https://doi.org/10.1002/jgrc.20217
Sheen, K. L., Brearley, J. A., Naveira Garabato, A. C., Smeed, D. A., Laurent, L. S., Meredith, M. P., et al. (2015). Modification of turbulent dissipation rates by a deep Southern Ocean eddy. *Geophysical Research Letters*, *42*, 3450–3457. https://doi.org/10.1002/2015GL063216
Siegelman, L., Klein, P., Riviere, P., Thompson, A. F., Torres, H. S., Flexas, M., & Menemenlis, D. (2020). Enhanced upward heat transport at deep submesoscale ocean fronts. *Nature Geoscience*, *13*, 50–55. https://doi.org/10.1038/s41561-019-0489-1
Smith, W. H. F., & Sandwell, D. T. (1997). Global sea floor topography from satellite altimetry and ship depth soundings. *Science*, *277*, 1956–1962. https://doi.org/10.1126/science.277.5334.1956
St. Laurent, L. C., Simmons, H. L., & Jayne, S. R. (2002). Estimating tidally driven mixing in the deep ocean. *Geophysical Research Letters*, *29*, 2106. https://doi.org/10.1029/2002GL015633
St. Laurent, L., Naveira Garabato, A. C., Ledwell, J. R., Thurnherr, A. M., Toole, J. M., & Watson, A. J. (2013). Turbulence and diapycnal mixing in Drake Passage. *Journal of Physical Oceanography*, *42*, 2143–2152. https://doi.org/10.1175/JPO-D-12-027.1
Takahashi, A., & Hibiya, T. (2019). Assessment of finescale parameterizations of deep ocean mixing in the presence of geostrophic current shear: Results of microstructure measurements in the Antarctic Circumpolar Current region. *Journal of Geophysical Research: Oceans*, *124*, 135–153. https://doi.org/10.1029/2018JC014030
Thomas, L. N., & Taylor, J. R. (2014). Damping of inertial motions by parametric subharmonic instability in baroclinic currents. *Journal of Fluid Mechanics*, *743*, 280–294. https://doi.org/10.1017/jfm.2014.29
Trossman, D. S., Waterman, S., Polzin, K. L., Arbic, B. K., Garner, S. T., Naveira-Garabato, A. C., & Sheen, K. L. (2015). Internal lee wave closures: Parameter sensitivity and comparison to observations. *Journal of Geophysical Research: Oceans*, *120*, 7997–8019. https://doi.org/10.1002/2015JC010892
Waterhouse, A. F., MacKinnon, J. A., Nash, J. D., Alford, M. H., Kunze, E., Simmons, H. L., et al. (2014). Global patterns of diapycnal mixing from measurements of the turbulent dissipation rate. *Journal of Physical Oceanography*, *44*(7), 1854–1872. https://doi.org/10.1175/JPO-D-13-0104.1
Waterman, S., Naveira Garabato, A. C., & Polzin, K. L. (2013). Internal waves and turbulence in the Antarctic Circumpolar Current. *Journal of Physical Oceanography*, *43*, 259–282. https://doi.org/10.1175/JPO-D-11-0194.1
Waterman, S., Polzin, K. L., Naveira Garabato, A. C., Sheen, K. L., & Forryan, A. (2014). Suppression of internal wave breaking in the Antarctic Circumpolar Current near topography. *Journal of Physical Oceanography*, *44*, 1466–1492. https://doi.org/10.1175/JPO-D-12-0154.1
Whitt, D. B., & Thomas, L. N. (2013). Near-inertial waves in strongly baroclinic currents. *Journal of Physical Oceanography*, *43*, 706–725. https://doi.org/10.1175/JPO-D-12-0132.1

Yang, L., Nikurashin, M., Hogg, A. M., & Sloyan, B. M. (2018). Energy loss from transient eddies due to lee wave generation in the Southern Ocean. *Journal of Physical Oceanography*, *48*, 2867–2885. https://doi.org/10.1175/JPO-D-18-0077.1

Zheng, K., & Nikurashin, M. (2019). Downstream propagation and remote dissipation of internal waves in the Southern Ocean. *Journal of Physical Oceanography*, *49*, 1873–1887. https://doi.org/10.1175/JPO-D-18-0134.1